(Received 22 October 2025, Accepted 8 December 2025, Scheduled 18 December 2025)

Compact Gap-Coupled Circularly Polarized Broadband Metasurface Antenna Based on Characteristic Mode Analysis

Xuemei Zheng[1] and Ao Gui[2,*]

[1]*Key Laboratory of Modern Power System Simulation and Control and Renewable Energy Technology Ministry of Education, Northeast Electric Power University, Jilin, China*
[2]*Northeast Electric Power University, Jilin, China*

ABSTRACT: In response to the demand for broadband antennas in satellite communications, this paper sets out the proposal of a broadband circularly polarised metasurface antenna. Based on the theory of characteristic mode analysis of super surface, a pair of characteristic modes with the potential to realize circular polarization broadband are obtained and used as the modes to be excited. At the same time, the metasurface current is analyzed; the position of the floor gap is determined according to the results; and the shape of the floor gap is designed to better stimulate the characteristic mode. Subsequently, the power is transmitted through the microstrip line gap coupling feeding structure to excite the selected mode. Finally, an MTS antenna with dimensions of $0.9\lambda_0 \times 0.9\lambda_0 \times 0.076\lambda_0$ at a centre frequency of 5 GHz was determined. The antenna was modeled using CST, a 3D electromagnetic simulation software, and then physically tested for verification. The experimental findings indicate that the impedance bandwidth of the antenna in question is 4.20–5.83 GHz (relative bandwidth of 32.6%). Furthermore, the 3 dB axial ratio bandwidth is 4.38–5.97 GHz (relative bandwidth of 30.7%).

1. INTRODUCTION

The antenna is composed of metasurface composed of triangular elements and a slit floor, as well as microstrip lines. With the rapid development of wireless communication technology, especially in 5G and the upcoming 6G communication networks, efficient and compact antenna design [1, 2] has become the key to ensuring communication quality and system capacity. Circularly polarized antennas play an important role in various wireless communications, satellite communications, radars and positioning systems because they can resist multipath effects and polarization mismatches. However, traditional circularly polarized antennas have the characteristics of narrow bands and high profiles, which will limit their application in the field of wireless communication. People have attempted to optimize the performance of circularly polarized broadband by adopting methods such as parasitic patches [3], adding air layers [4], multi-feed networks [5], and multi-layer patch structures [6]. However, these methods still have characteristics such as high contour structure and complex structure. The antenna proposed in [7] is fed with coplanar waveguide. This feeding method achieves a low profile while expanding the circularly polarized bandwidth; however, the radiation gain of this structure is very low.

Metasurfaces (MTSs) are a type of two-dimensional material composed of a set of structural units, usually tiny metallic or dielectric components, and many researchers [8–15] have designed the shape, size, and arrangement of these units to improve the bandwidth and polarization properties of antennas. Study [8] demonstrates that the 4×4 dual-layer metasurface significantly enhances the bandwidth of microstrip patch antennas, achieving impedance matching across a wide band from 4.7 to 6.66 GHz. The MTS proposed in [9] consists of tangential square elements, achieving an impedance matching bandwidth (IBW) of -10 dB at 4.42–6.22 GHz and an axial ratio (AR) bandwidth of 3 dB at 4.60–5.72 GHz. The MTS proposed in [10] adopts rectangular elements and achieves a 3 dB axial ratio bandwidth (ARBW) of 3.75–4.85 GHz. The design of MTS enables these antennas to achieve circularly polarised broadband. However, the adoption of a dual-port power supply configuration resulted in a relatively complex overall structure. The complexity of these structures invariably increases the difficulty and cost of their manufacture. The work [11] achieved a 3 dB axial ratio bandwidth of 20.01% (14.05–172 GHz) by employing a dual-layer metasurface structure. Meanwhile, study [12] utilized a 2×2 metasurface to realize circular polarization (CP) characteristics with an ARBW of 12.9%. Many researchers have also used the characteristic mode theory to design broadband antennas [16–19]. In [16], researchers applied characteristic mode theory to design a monopole-based ultra-wideband (UWB) antenna, achieving broadband impedance matching across 3.03–11.75 GHz. Ref. [17] utilized characteristic mode analysis to design a racquet-shaped UWB multiple-input multiple-output (MIMO) antenna, realizing broadband impedance matching from 3 to 21 GHz. Ref. [18] validated dual-band broadband antenna designs through characteristic mode analysis, achieving impedance matching bands of 5.2–5.8 GHz and 7.9–8.4 GHz, respectively. Ref. [19] implemented dual-band performance using metasurfaces, with frequency bands of 4.13–5.94 GHz and 7.6–8.4 GHz. Ref. [20] demonstrated circularly polarized broadband through slot-coupled mi-

* Corresponding author: Ao Gui (2202300384@neepu.edu.cn).

crostrip line feeding structures, achieving an aspect ratio bandwidth of 26.4% (3.58–40.67 GHz), showcasing the effectiveness of slot-coupled feeding methods in circularly polarized broadband antenna applications. Moreover, despite the success of diverse methodologies in achieving specific outcomes, the ongoing challenge remains unresolved: the necessity to expand the operational frequency range while maintaining circular polarization performance and to streamline the design.

This study proposes a design methodology for a circularly polarised broadband antenna based on MTS, using a slot-coupled microstrip feed approach. Its radiative layer is composed of multiple sub-wavelength metal patch units. By optimizing these non-periodically arranged units, the effective control over the polarization state of electromagnetic waves is achieved. Despite the use of a non-periodic structure, this MTS design approach fully conforms to the core definition and design paradigm of metasurfaces [21–23]. First, characteristic modes and surface currents of the MTS are analysed by characteristic mode theory, and the characteristic modes with mutually perpendicular modal current directions are selected as the working modes. Then, the positions of the ground plane slots are determined based on the distribution of the characteristic current intensity of the MTS. By designing ground plane slots, the effective excitation of working modes is achieved. Ultimately, this study can significantly improve the bandwidth and polarisation performance of the antenna while maintaining a compact structure. In addition, the professional electromagnetic simulation software CST is used for simulation experiments to ensure that the designed antenna has accurate experimental results.

2. CHARACTERISTIC MODE ANALYSIS (CMA)

In recent years, characteristic mode theory has been used as a new and effective method for internal work mechanism analysis and MTS antenna design [24–27]. Characteristic Mode Theory (CMT) decomposes the electromagnetic response of the structure into a set of basic characteristic modes.

By analysing each characteristic mode's surface current, the MTS can be specifically designed. The surface current of an ideal conductor is defined as follows:

$$J = \sum_n a_n J_n \tag{1}$$

J_n is the Nth mode ($n = 0, 1, 2, 3, \ldots$), the characteristic currents in it. a_n is referred to as the modal excitation coefficient of the Nth characteristic mode. J is the total characteristic surface current. Modal Significance (MS) indicates the extent to which each characteristic current is easily excited and is related only to the conductor itself, rather than whether the conductor is excited or not. Mode significance indicates the extent to which each characteristic current is easily excited. If $MS_n = 1$, it is in resonant mode; if $MS_n = 0$, it is in non-resonant mode. In general, the frequency range with $MS_n > 0.707$ is taken as the resonant frequency band. The MS_n formula is as follows::

$$MS_n = 1/|1 + j\lambda_n| \tag{2}$$

Normally, at least two modes are required to achieve CP radiation using characteristic modes. It means that two resonant modes should be excited within the same frequency band, each with a 90° phase difference [26, 27], or a feed structure should be used to obtain a 90° phase difference [24, 25]. In this paper, a feeder structure is chosen to realize CP radiation.

3. ANTENNA DESIGN

3.1. Design of MTS Based on Characteristic Modes

The overall structure of the antenna designed in this article is shown in Fig. 1. The upper and lower dielectric layers are made of Fr4 material with relative dielectric constant 4.4. First, the characteristic mode analysis of the MTS is performed using the CST simulation software.

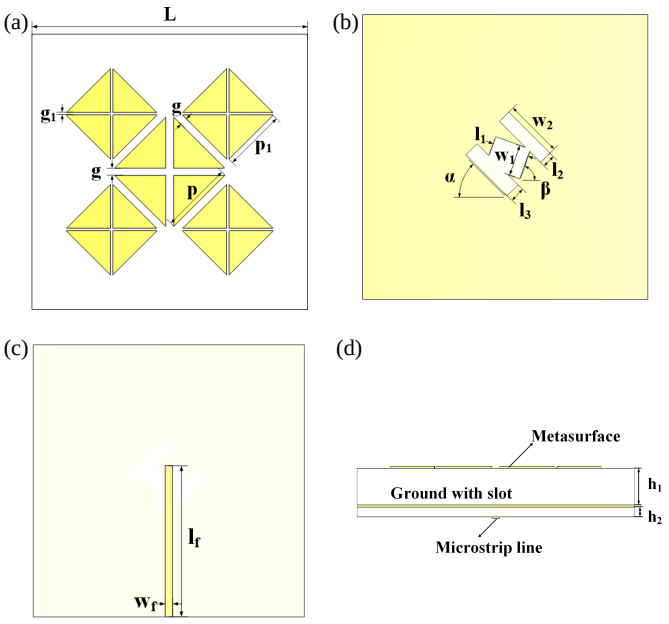

FIGURE 1. Configuration of the MTS antenna. (a) Top view of the proposed MTS, (b) floor gaps, (c) back view of microstrip line, (d) side view.

As shown in Fig. 2(a), it is composed of four triangular patch units. The triangular units are sub-wavelength and are designed to achieve special electromagnetic characteristics. The overall structure and design purpose conform to the broad definition of MTS. Similarly, the patches in Fig. 2(b) add two-dimensional

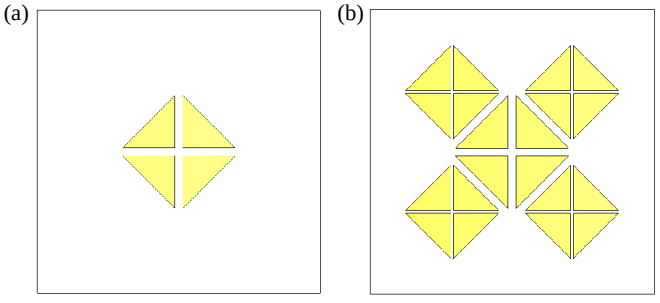

FIGURE 2. (a) Initial MTS, (b) the proposed MTS.

surrounding patches to the patches shown in Fig. 2(a), so this patch array also belongs to MTS.

First, an initial MTS as shown in Fig. 2(a) was designed. The surface current and three-dimensional radiation patterns of this MTS were analyzed to obtain the distribution of the MTS characteristic currents as shown in Fig. 3 and the three-dimensional radiation patterns of various modes as shown in Fig. 5. As shown the three-dimensional radiation diagram in Fig. 5, red represents high radiation intensity, and the lighter the colour, the lower the radiation intensity. It can be clearly seen that mode1 (M_1) and mode2 (M_2) have very high radiation intensities along the $+Z$ axis (towards us), while M_3 and M_4 have very low radiation intensities along the $+Z$ axis. In addition, the radiation directions of M_1 and M_2 point only towards the $+Z$ axis, while those of mode3 (M_3) and mode4 (M_4) point in all directions. The radiation direction required in this study is exactly a single direction. However, as shown in Fig. 3, the current distribution positions of Modes 1 to 4 are very close to each other. This situation will cause great difficulties in designing the feed structure to excite the required modes (M_1, M_2). Therefore, as shown in Fig. 2(b), the patch designed in this paper is placed around the initial MTS to alter the current distribution of the characteristic mode. Fig. 4 shows the mode current distribution of MTS after adding the parasitic patches. The mode currents J_1 and J_2 are in phase across the entire MTS, polarized along $+45°$ and $-45°$ directions respectively. Their maximum current distributions concentrate at both the central patch and its edge areas. The two modes exhibit identical mode importance values [see Fig. 6] and orthogonal radiation patterns [see Fig. 5]. In contrast, mode currents J_3 and J_4 are out of phase, with their maximum currents distributed at the parasitic patches. Therefore, modes J_1 and J_2 are selected as candidates for generating CP radiation. It is clearly distinguishable that the surface current distributions of M_1 and M_2 remain on the initial MTS, while the current distributions of M_3 and M_4 are dispersed onto the surrounding patches, and the current intensity of the central patch is very small. Although the proposed metasurface exhibits altered current patterns compared to the original design, its three-dimensional radiation distribution remains essentially consistent [see Fig. 5]. Based on the above mode current analysis, the feed structure design in the central area of MTS can effectively stimulate M_1 and M_2, while reducing the interference of M_3 and M_4.

According to [24] and [25], as shown in Fig. 6, the MS of M_1 and M_2 overlap each other, i.e., these two modes form a pair of degenerate modes, and a phase difference of 90 degrees between M_1 and M_2 is generated through the design of the feed to achieve circular polarization radiation. To achieve circularly polarised broadband by using two modes, it is required that the resonant frequencies of these two modes are similar, and a pair of degenerate modes is a very good choice. The MS curves of M_1 and M_2 are greater than 0.7, indicating a broadband above 1 GHz. It suggests that M_1 and M_2 can be easily excited in this frequency band to achieve broadband performance. The MS curves of M_3 and M_4 in Fig. 6 also show broadband characteristics. The MS bandwidth of M_1 and M_2 overlaps with that of M_3 and M_4. Therefore, in the same frequency band, M_1 and M_2 can be excited, while M_3 and M_4 will cause interference, affecting the performance of the broadband generated by M_1 and M_2. However, through the analysis of the surface currents of the above four characteristic modes, the design of the feed position at the center of MTS can effectively stimulate M_1 and M_2 while reducing the stimulation of M_3 and M_4. The following is the design of the feed structure to achieve this purpose.

3.2. Design of Feed Structure

Based on the surface current of the required characteristic mode of MTS obtained from the above text, the feeding structure must feed the MTS centre in order to excite M_1 and M_2 and suppress M_3 and M_4. In this paper, the gap coupling feeding method is chosen for feeding. This feeding method can excite the MTS well and ensure the radiation gain of the antenna. The shape of the gaps on the ground determines the excitation effect for MTS.

The design of floor gaps is the key to gap coupling feeding. As shown in Fig. 1(b), the floor gap consists of three rectangular sections: a central rectangular gap and two parallel rectangular gaps surrounding it. α represents the angle between the two parallel rectangular gaps and the horizontal line, while β denotes the angle between the central gap and the horizontal line. By adjusting α, the impedance matching bandwidth and circular polarization bandwidth performance of the antenna can be effectively adjusted. The overall parameters of the antenna are given in Table 1. As shown in Fig. 7(a), as α increases, the IBW also increases. It is observed in Fig. 7(b) that only $\alpha = 45°$ achieves the ARBW.

TABLE 1. Dimensions of the optimized antenna structure. (Unit: mm)

Parameters	Numerical value	Parameters	Numerical value
L	54	w_1	6
h_1	4	w_2	11
h_2	0.5	l_1	6
p	10	l_2	2.5
p_1	8.6	w_f	1.5
g	1.5	l_f	30
g_1	0.5	β	70°
α	45°		

Another parameter of the floor gap that greatly affects the impedance and 3 dB ARBW is the rotation angle of central rectangular gap β, as illustrated in Fig. 8. It is seen that a good impedance and 3 dB AR bandwidths can be obtained by adjusting β to 70°. It can be seen that the operation of rotating the central rectangular gap effectively improves the impedance and circular polarisation performance of the antenna.

As shown in Fig. 1(b), the width parameter w_1 of the central rectangle in the floor gap structure significantly affects the overall floor gap area. The following analysis examines w_1's influence on the antenna's broadband performance. First, according to the S-parameter results in Fig. 9(a), increasing w_1 slightly expands the impedance-matched bandwidth. Compared with the AR curve results in Fig. 9(b), at $w_1 = 5.5$,

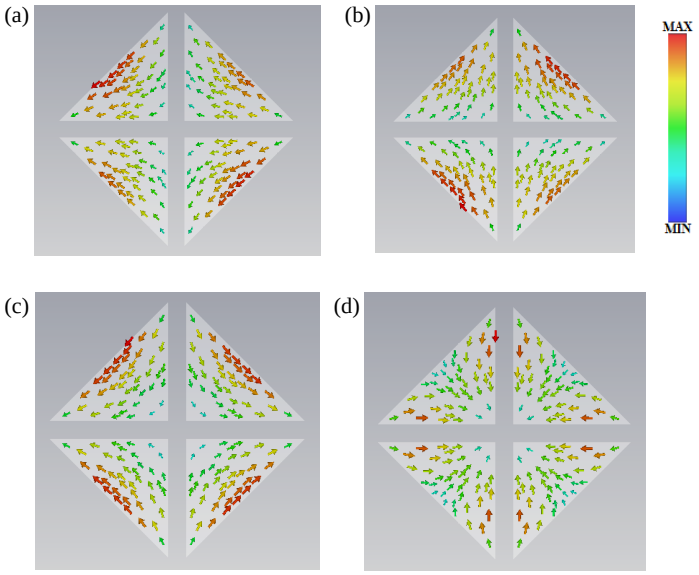

FIGURE 3. Initial MTS current of the first four modes: (a) J_1, (b) J_2, (c) J_3, (d) J_4.

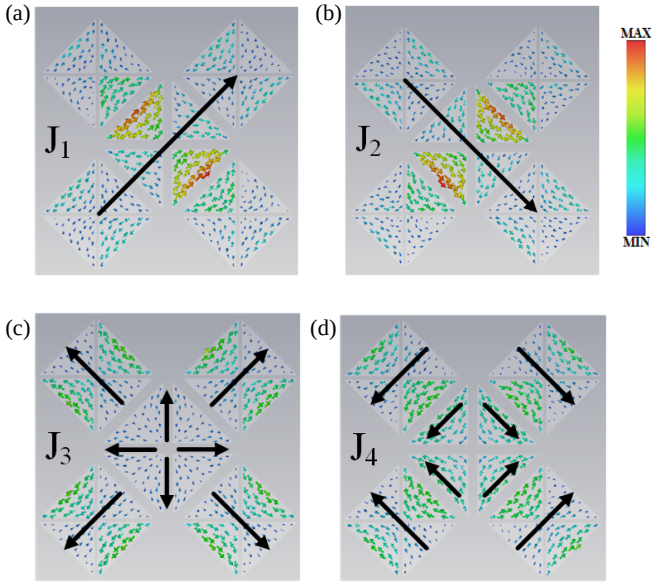

FIGURE 4. The proposed MTS current of the first four modes: (a) J_1, (b) J_2, (c) J_3, (d) J_4.

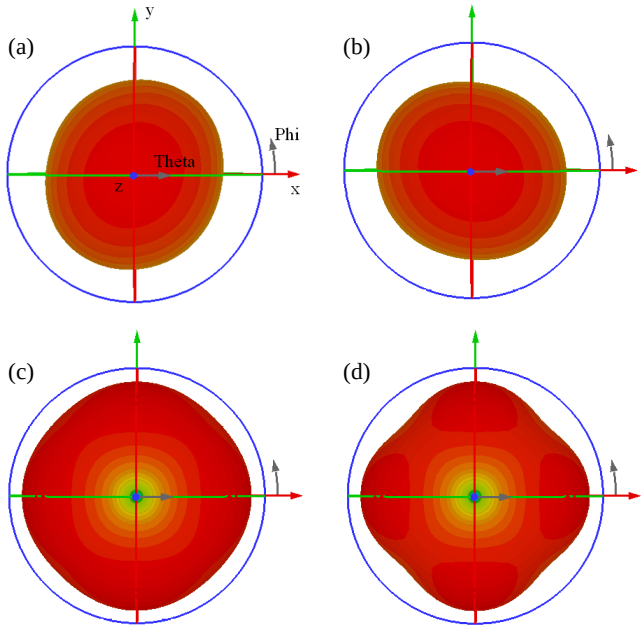

FIGURE 5. Four mode radiation patterns of the initial metasurface and the proposed metasurface: (a) M_1, (b) M_2, (c) M_3, (d) M_4.

the 3 dB bandwidth is only 0.5 GHz. When $w_1 = 6.0$, the AR below 3 dB drops significantly, approaching 0 dB near 5.1 GHz, while the overall AR bandwidth reaches 1.49 GHz. At $w_1 = 6.5$, the AR value at 4.7 GHz exceeds 3 dB, and the frequency range with AR below 3 dB shifts to higher frequencies, deviating from the impedance-matched bandwidth range shown in Fig. 9(a), resulting in poorer overall antenna performance. Comprehensive analysis of w_1 parameters indicates that $w_1 = 6.0$ meets the broadband performance requirements for circular polarization in this study.

The microstrip line dimensions are critical parameters affecting antenna performance. The analysis of the microstrip line length (l_f) in Fig. 1(c) reveals that: When $l_f = 28$, the antenna fails to achieve impedance matching and circular polarization broadband performance as shown in Figs. 10(a) and (b). At $l_f = 32$, while demonstrating good impedance matching broadband performance, the performance of circular polarization in the wideband is generally average (ARBW < 0.5 GHz). However, at $l_f = 30$, the antenna exhibits excellent performance in both impedance matching and circular polarization broadband. Therefore, this paper adopts $l_f = 30$ as the final parameter for the microstrip line length.

4. EXPERIMENTAL RESULTS AND COMPARISONS

4.1. Experimental Simulation Results

To verify the simulation's feasibility, we fabricated an MTS antenna prototype and conducted field tests using a vector network analyzer. Fig. 11 shows a photograph of the fabricated antenna including two layers of FR-4 dielectric plates for the MTS and feed structure, with the MTS copper side on the top surface, the middle surface of the two dielectric plates for the floor slit structure, and the microstrip line on the bottom surface.

The simulation and measurement results of the proposed MTS antenna are shown in Fig. 12. The S-parameter is used to measure the impedance matching bandwidth, and the results of the S-parameter can be measured using a vector network analyser. The simulation result of the S-parameter bandwidth of this antenna -10 dB is $4.20 \sim 5.83$ GHz, with a relative bandwidth of 32.6%, and the actual measured IBW is basically consistent with the simulation result. The processing and measurement errors will lead to a slight shift between the measured and simulated results. The deviation may be caused by the loss

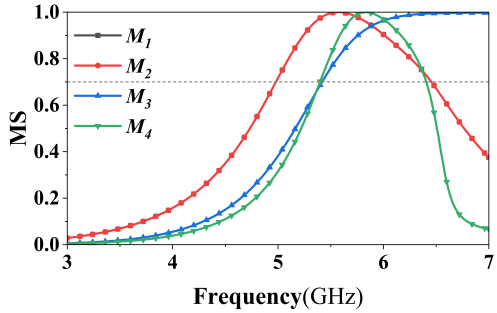

FIGURE 6. Modal significances of the proposed MTS.

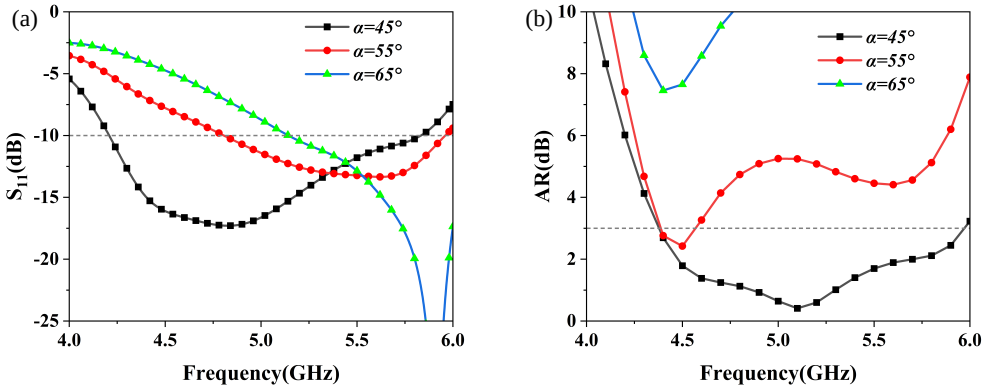

FIGURE 7. Effect of rotated angle α on (a) S_{11} and (b) AR.

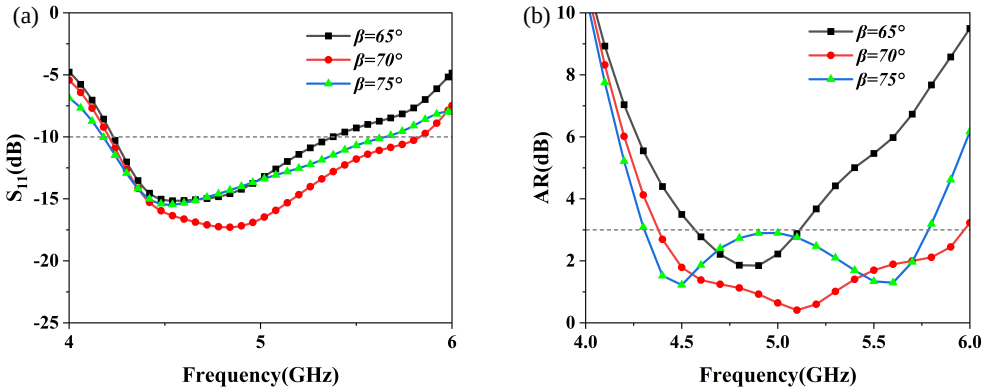

FIGURE 8. Effect of rotated angle β on (a) S_{11} and (b) AR.

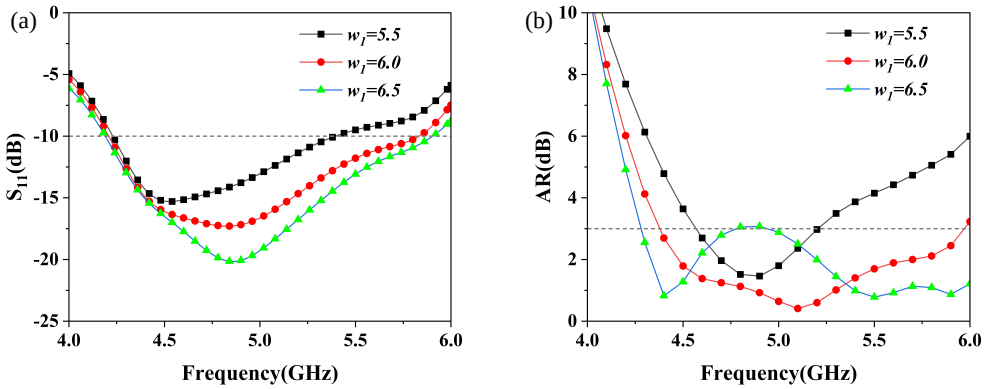

FIGURE 9. Effect of w_1 on (a) S_{11} and (b) AR.

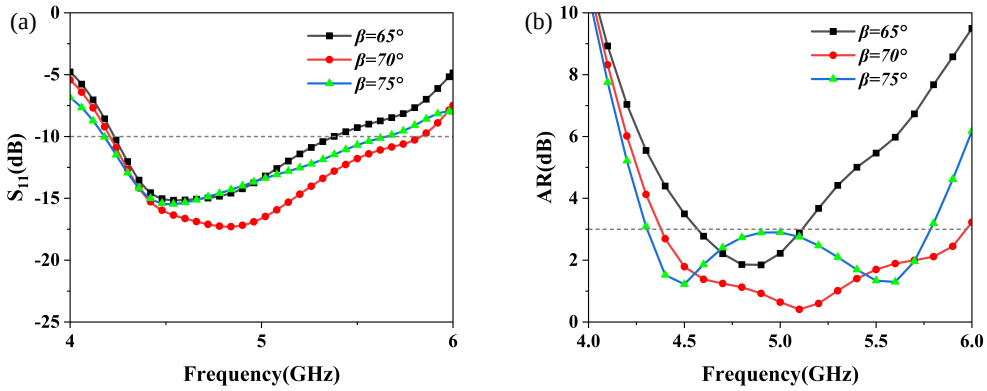

FIGURE 10. Effect of l_f on (a) S_{11} and (b) AR.

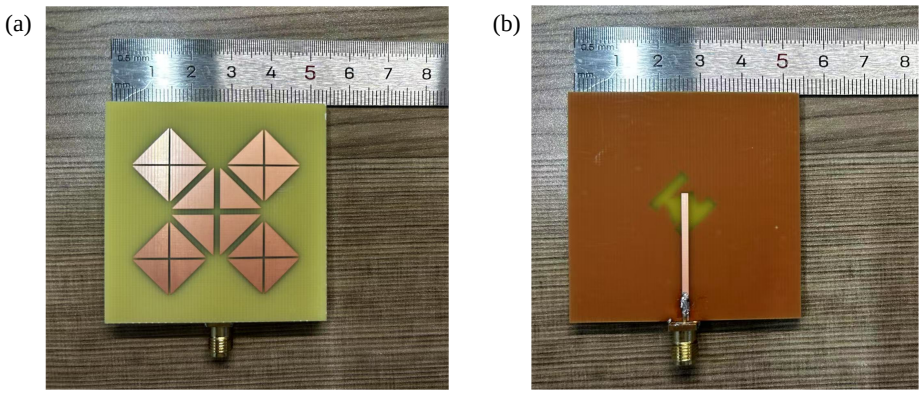

FIGURE 11. Photographs of the fabricated antenna sample. (a) Front view, (b) back view.

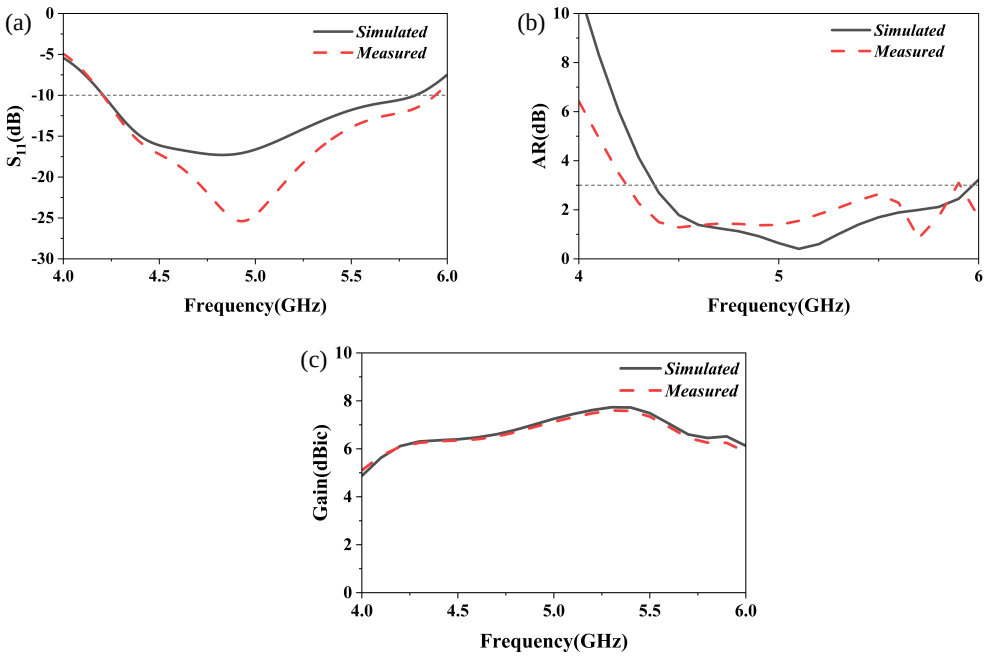

FIGURE 12. The proposed antenna: (a) reflection coefficient (S_{11}), (b) AR, (c) gain.

of the cable used in the actual measurement and the error of the circuit board processing, which are difficult to simulate by CST software. ARBW is a measure of circularly polarised bandwidth, and a bandwidth of less than 3 dB is generally regarded as circularly polarised bandwidth. Fig. 12(b) shows the comparison between the measured and simulated results of the 3 dB ARBW of the antenna. Fig. 13 shows the comparison between the measured and simulated results of the antenna's left circu-

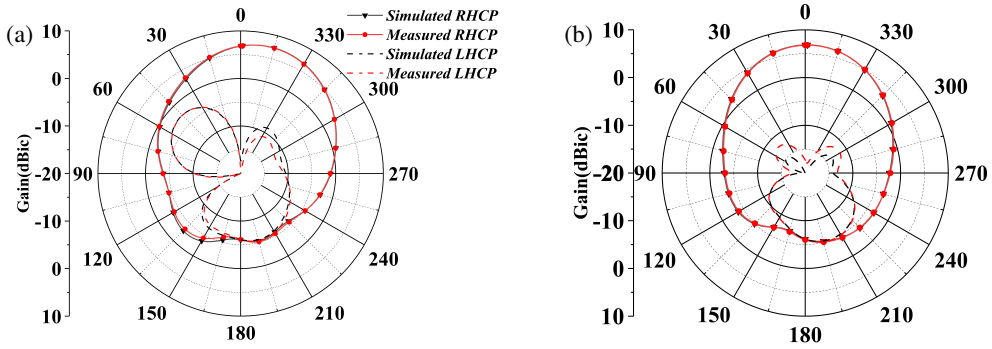

FIGURE 13. Radiation patterns of the proposed MTS antenna. (a) E plane and (b) H plane at 5 GHz.

larly polarized (LHCP) and right circularly polarized (RHCP) polar radiation patterns for the E-plane and H-plane at the centre frequency of 5 GHz, which shows that the antenna is circularly polarized as RHCP, and the radiation direction is concentrated in the z-axis, which is in line with the expected radiation performance. The measured results are basically consistent with the simulated ones, which verifies the feasibility of the antenna design.

4.2. Comparative Analysis of CP Antenna

The performance comparison between the antenna designed in this paper and the antenna in the reference literature is presented in Table 2. The antenna proposed in [7] is very small in size and wide in bandwidth, but its gain is lower than that of the antenna proposed in this paper, and its operating frequency is not the C-band commonly used in satellite communication. The operating frequencies of these antennas proposed in [9, 10] are relatively close to those proposed in this paper, all in the C-band. The antenna proposed in [9] has high gain, but its size is relatively large, which limits its application scenarios. The antenna proposed in [10] has a gain similar to that of the antenna in this paper, but the ARBW performance of the antenna proposed in this paper is 7.2% higher than that of the antenna in the previous reference. The antenna proposed in [13] is very small in size, but its impedance matching bandwidth and circular polarization bandwidth are much narrower than those of the antenna proposed in this paper. Although the impedance matching bandwidth of [14, 15] is similar to that of this antenna, the ARBW is significantly narrower than that of this antenna. Refs. [26, 27] also employed CMA for antenna design. Compared with these two antennas, the antenna proposed in this paper has a significant advantage in circular polarization broadband performance. The overlap bandwidth between impedance-matched broadband and circularly polarized broadband is also a key metric for evaluating operational bandwidth. The proposed antenna overlapping broadband in this paper has the largest relative broadband in Table 2, thus showing excellent working broadband. The designed antenna achieves the coordinated optimization of wideband circular polarization and high gain under a compact size, providing a miniaturized and high-performance antenna solution for satellite navigation systems.

TABLE 2. Comparison of antenna performance with literature.

Ref.	Sizes (λ_n^3)	IBW (%)	ARBW (%)	Overlapping Bandwidth (%)	Peak Gain (dBic)
[7]	$0.15 \times 0.15 \times 0.1$	47	34.7	23.1	3.4
[9]	$1.4 \times 1.4 \times 0.69$	36	22.4	22.4	11.22
[10]	$1.12 \times 0.86 \times 0.069$	31	25.6	25.6	7.4
[13]	$0.38 \times 0.38 \times 0.066$	15.7	11	11	5.5
[14]	$0.92 \times 0.92 \times 0.076$	33.6	19.4	19.4	9
[15]	$0.6 \times 0.49 \times 0.07$	33.7	16.5	16.5	5.8
[26]	$1.5 \times 1.5 \times 0.061$	38.8	14.3	14.3	9.4
[27]	$0.24 \times 0.24 \times 0.115$	N/A	N/A	21.1	7.4
Prop.	$0.9 \times 0.9 \times 0.076$	32.6	30.7	29	7.6

5. CONCLUSION

This paper proposes an MTS slit coupling feed antenna. The MTS is a brand new structure composed of triangular elements, and the mode analysis is performed by CMT. The mode to be excited is selected based on the MS curve and three-dimensional radiation map. Then, the feeding position at the centre of the MTS is determined based on the characteristic current distribution of the MTS. Finally, a novel floor-gap feeding structure was set up, and the microstrip feeding method was adopted. Time domain simulation was then performed to achieve good impedance matching and circularly polarised broadband performance. This antenna is designed for MTS, which provides a good solution for the design of circularly polarised antennas and the realisation of the design of MTS excitation-gap coupling feeding structure. The antenna broadband frequency band proposed in this paper is located in the core area of the C-band and can have good application scenarios in the fields of wireless communication and satellite communication.

REFERENCES

[1] Fan, F.-F., Q.-L. Chen, Y.-X. Xu, X.-F. Zhao, J.-C. Feng, and Z.-H. Yan, "A wideband compact printed dipole antenna array with SICL feeding network for 5G application," *IEEE Antennas and*

Wireless Propagation Letters, Vol. 22, No. 2, 283–287, 2023.
[2] Nie, L. Y., B. K. Lau, S. Xiang, H. Aliakbari, B. Wang, and X. Q. Lin, "Wideband design of a compact monopole-like circular patch antenna using modal analysis," *IEEE Antennas and Wireless Propagation Letters*, Vol. 20, No. 6, 918–922, 2021.
[3] Tang, X., Y. He, and B. Feng, "Design of a wideband circularly polarized strip-helical antenna with a parasitic patch," *IEEE Access*, Vol. 4, 7728–7735, 2016.
[4] Liu, S., W. Wu, and D.-G. Fang, "Wideband monopole-like radiation pattern circular patch antenna with high gain and low cross-polarization," *IEEE Transactions on Antennas and Propagation*, Vol. 64, No. 5, 2042–2045, May 2016.
[5] Lin, C., F.-S. Zhang, Y.-C. Jiao, F. Zhang, and X. Xue, "A three-fed microstrip antenna for wideband circular polarization," *IEEE Antennas and Wireless Propagation Letters*, Vol. 9, 359–362, 2010.
[6] Ding, K., Y. Wu, K.-H. Wen, D.-L. Wu, and J.-F. Li, "A stacked patch antenna with broadband circular polarization and flat gains," *IEEE Access*, Vol. 9, 30 275–30 282, 2021.
[7] Cao, R. and S.-C. Yu, "Wideband compact CPW-fed circularly polarized antenna for universal UHF RFID reader," *IEEE Transactions on Antennas and Propagation*, Vol. 63, No. 9, 4148–4151, 2015.
[8] Yang, K., M. Wang, and X. Jia, "Improved bandwidth of patch antenna using dual-layer metasurface," *Progress In Electromagnetics Research Letters*, Vol. 124, 69–75, 2025.
[9] Yang, W., Q. Meng, W. Che, L. Gu, and Q. Xue, "Low-profile wideband dual-circularly polarized metasurface antenna array with large beamwidth," *IEEE Antennas and Wireless Propagation Letters*, Vol. 17, No. 9, 1613–1616, Sep. 2018.
[10] Zeng, Y., X. Qing, and M. Y.-W. Chia, "A wideband circularly polarized antenna with a nonuniform metasurface designed via multiobjective bayesian optimization," *IEEE Antennas and Wireless Propagation Letters*, Vol. 23, No. 6, 1739–1743, Jun. 2024.
[11] Wan, W., W. Ji, Z. Wang, and X. Jiang, "Wideband circularly polarized dielectric resonator antenna based on double-layer metasurface," *Progress In Electromagnetics Research C*, Vol. 158, 197–203, 2025.
[12] Geng, G. and Z. Ding, "Wideband metasurface antenna with polarization reconfigurable controlled by resistors," *Progress In Electromagnetics Research Letters*, Vol. 127, 15–21, 2025.
[13] Nasimuddin, and X. Qing, "A miniaturized wideband circularly polarized antenna using metasurface," in *2022 16th European Conference on Antennas and Propagation (EuCAP)*, 1–5, Madrid, Spain, 2022.
[14] Ding, K., R. Hong, D. Guan, L. Liu, and Y. Wu, "Broadband circularly polarised stacked antenna with sequential-phase feed technique," *IET Microwaves, Antennas & Propagation*, Vol. 14, No. 8, 779–784, 2020.
[15] Wu, Z., L. Li, Y. Li, and X. Chen, "Metasurface superstrate antenna with wideband circular polarization for satellite communication application," *IEEE Antennas and Wireless Propagation Letters*, Vol. 15, 374–377, 2015.
[16] Xiang, Z., Z. Wang, C. Li, and R. You, "Design of UWB monopole antenna with ring structure based on characteristic mode theory," *Progress In Electromagnetics Research C*, Vol. 158, 225–234, 2025.
[17] Wang, Z., F. Zhang, W. Nie, M. Yang, and C. Li, "A racket-shaped UWB MIMO antenna based on characteristic mode analysis," *Progress In Electromagnetics Research B*, Vol. 114, 37–50, 2025.
[18] Shahpari, A. and M. Shafeghati, "A new design of tunable dual band-notched UWB flower-shaped antenna verified by CMA," *Progress In Electromagnetics Research C*, Vol. 156, 217–225, 2025.
[19] Feng, H., Z. Wang, W. Nie, and M. Yang, "High-gain dual-band metasurface MIMO antenna for enhanced 5G and satellite applications," *Progress In Electromagnetics Research C*, Vol. 156, 13–22, 2025.
[20] Ji, W., Y. Gao, X. Jiang, X. Li, and W. Wan, "A circularly polarized magnetoelectric dipole antenna with microstrip-line aperture-coupled feeding," *Progress In Electromagnetics Research C*, Vol. 154, 11–19, 2025.
[21] Shang, S., F. Tang, X. Ye, Q. Li, H. Li, J. Wu, Y. Wu, J. Chen, Z. Zhang, Y. Yang, and W. Zheng, "High-efficiency metasurfaces with 2π phase control based on aperiodic dielectric nanoarrays," *Nanomaterials*, Vol. 10, No. 2, 250, 2020.
[22] Wang, Y., K. Chen, Y. Li, and Q. Cao, "Design of nonresonant metasurfaces for broadband RCS reduction," *IEEE Antennas and Wireless Propagation Letters*, Vol. 20, No. 3, 346–350, 2021.
[23] Zhang, Q., X. Wan, S. Liu, J. Y. Yin, L. Zhang, and T. J. Cui, "Shaping electromagnetic waves using software-automatically-designed metasurfaces," *Scientific Reports*, Vol. 7, No. 1, 3588, 2017.
[24] Gao, X., G. Tian, Z. Shou, and S. Li, "A low-profile broadband circularly polarized patch antenna based on characteristic mode analysis," *IEEE Antennas and Wireless Propagation Letters*, Vol. 20, No. 2, 214–218, Feb. 2021.
[25] Liu, S., D. Yang, and J. Pan, "A low-profile broadband dual-circularly-polarized metasurface antenna," *IEEE Antennas and Wireless Propagation Letters*, Vol. 18, No. 7, 1395–1399, Jul. 2019.
[26] Zhao, C. and C.-F. Wang, "Characteristic mode design of wide band circularly polarized patch antenna consisting of H-shaped unit cells," *IEEE Access*, Vol. 6, 25 292–25 299, 2018.
[27] Zeng, J., X. Liang, L. He, F. Guan, F. H. Lin, and J. Zi, "Single-fed triple-mode wideband circularly polarized microstrip antennas using characteristic mode analysis," *IEEE Transactions on Antennas and Propagation*, Vol. 70, No. 2, 846–855, Feb. 2022.